Electronic structure and excitations in oxygen deficient $CeO_{2-\delta}$ from DFT calculations

T. Jarlborg[1], B. Barbiellini[2], C. Lane[2], Yung Jui Wang[2,3], R.S. Markiewicz[2], Zhi Liu[3], Zahid Hussain[3] and A. Bansil[2]
[1] *DPMC, University of Geneva, 24 Quai Ernest-Ansermet, CH-1211 Geneva 4, Switzerland*
[2] *Department of Physics, Northeastern University, Boston, Massachusetts 02115, USA*
[3] *Advanced light Source, Lawrence Berkeley National Laboratory, Berkeley, California 94720, USA*

arXiv:1403.7650v1 [cond-mat.mtrl-sci] 29 Mar 2014

The electronic structures of supercells of $CeO_{2-\delta}$ have been calculated within the Density Functional Theory (DFT). The equilibrium properties such as lattice constants, bulk moduli and magnetic moments are well reproduced by the generalized gradient approximation (GGA). Electronic excitations are simulated by robust total energy calculations for constrained states with atomic core holes or valence holes. Pristine ceria CeO_2 is found to be a non-magnetic insulator with magnetism setting in as soon as oxygens are removed from the structure. In the ground state of defective ceria, the Ce-f majority band resides near the Fermi level, but appears at about 2 eV below the Fermi level in photoemission spectroscopy experiments due to final state effects. We also tested our computational method by calculating threshold energies in Ce-M_5 and O-K x-ray absorption spectroscopy and comparing theoretical predictions with the corresponding measurements. Our result that f electrons reside near the Fermi level in the ground state of oxygen deficient ceria is crucial for understanding the catalytic properties of CeO_2 and related materials.

PACS numbers: 71.28.+d, 71.15.Mb 71.15.Qe 79.60.-i

I. INTRODUCTION

Mixed-valency cerium oxides (ceria) are technologically important materials [1–3] with remarkable properties that are useful for applications in heterogeneous chemical [4] and electrochemical catalysis [5–8]. In chemical catalysis, ceria is used as an active support. Ceria at an interface catalyzes surface reactions [9, 10], while the bulk material is used as an oxygen reservoir. In electrocatalysis, on the other hand, mixed ionic and electronic conductivity (with electrons localized around Ce) [11, 12] is essential for making ceria a potentially good electrode in solid oxide fuel cells [13–16] with an outstanding electrocatalytic activity even without any metal co-catalyst [17].

Ce^{3+} and oxygen vacancies are thought to be the active sites on ceria surfaces [18–20] in reactions such as hydrolysis, with the surface undergoing a Ce^{3+}/ Ce^{4+} redox cycle during the complete catalytic reaction. In the pristine CeO_2 compound, Ce atoms assume a +4 oxidation state, but the phase diagram of ceria contains a continuous range of partially reduced phases $CeO_{2-\delta}$ in which oxygen vacancies can be easily formed or eliminated. The formation of oxygen vacancies in $CeO_{2-\delta}$ results in changes in cerium oxidation state similar to those implicated in the cuprates [21]. Notably, the Ce valence and defect structure in ceria can change in response to physical parameters such as temperature, voltage, and oxygen partial pressure [6].

The nature of the Ce active site remains not well-understood because studies with ceria are complicated by the fact that the f electrons appear to be far from the Fermi level. The degree of participation of f-electrons in catalytic reactions [22–25] is therefore not clear, since the standard theory of catalysis heavily relies on localized d orbitals at the Fermi energy, E_F [26]. Fortunately, the computational description of perfect CeO_2 structure is not so complicated due to the absence of Ce $4f$ electrons in the insulating material [27, 28]. However, in $CeO_{2-\delta}$, when partially filled f orbitals are involved, the ground state predicted by the density-functional theory (DFT) clearly places the f electrons in narrow bands piled at E_F, interacting only weakly with other electrons. Since the elusive $\alpha-\gamma$-transition in pure Ce can be described quite accurately by temperature dependent DFT calculations in which vibrational, electronic and magnetic free energies are taken into account, [29], DFT should be expected to provide a reasonable description of ceria. In fact, corrections to the value of the chemical expansion coefficient α_c [30] have been explained via disorder and entropy effects enhancing lattice expansion [29] rather than via correlations beyond the Generalized Gradient Approximation (GGA) [31]. In sharp contrast, however, signatures of f bands are often found in spectroscopic measurements not at the Fermi energy E_F, as GGA predicts, but several eV's above or below E_F depending on the nature of the spectroscopy. These shortcomings may be cured in an advanced DFT approach [32], which includes relaxation energies relevant for excitation of occupied and empty states in various spectroscopic probes. These relaxation energies are of the order of the corrections obtained within quasi-particle schemes [33, 34] or modeled by adding a Hubbard U term [35]. Overall, the published studies that consider CeO_2 cover the range of U parameter between 2 and 8 eV, depending on the property of interest [36–42]. Many-body perturbation theory with U [43], self-interaction corrections [44], and hybrid DFT functionals have also been considered [45, 46]. In the present study, we explore the relaxation energy approach [32] to find a reasonable description of x-ray photoemission (XPS) as well as x-ray absorption spectroscopy (XAS) results in $CeO_{2-\delta}$.

An outline of this paper is as follows. In Sec. II, we present details of our electronic structure and total

energy computations for various CeO_x supercells where $x = 2 - \delta$. Results of the calculations are presented and compared with relevant experimental data in Sec. III, and the conclusions are given in Sec. IV.

II. EXPERIMENTAL SETUP AND METHOD OF CALCULATION

The photoelectron spectroscopy experiments were performed at beamline 9.3.2 at the Advanced Light Source (Berkeley). Detailed description of the AP-XPS endstation used in this study and the ceria thin films sample preparation can be found in Refs. 47 and 48. The Fermi level was determined by using a gold foil. The binding energy was also calibrated by using the Pt $4f$ core level. The Ce $4f$ spectrum was collected at a photon energy of 270 eV [49]. In the interest of brevity, we refer to previous publications for further details of measurements. [49, 50]

In order to determine various equilibrium properties, we used the pseudo-potential projected augmented wave method [51] implemented in the VASP package [52] with an energy cutoff of 520 eV for the plane-wave basis set. CeO_2 has a cubic fluorite lattice ($Fm\bar{3}m$) with four cerium and eight oxygen atoms per unit cell. The exchange-correlation energy was computed using the GGA functional [53], which gives a reasonable agreement with experimental low temperature equilibrium volumes for CeO_2 and Ce_2O_3. Andersson *et al.* [36] have pointed out that this agreement is not maintained if a non-zero Coulomb parameter U is deployed in the GGA scheme.

To estimate the XPS and XAS relaxation effects, we have performed self-consistent first-principles calculations using the the Linear Muffin-Tin Orbital (LMTO) method [54] within the Local Spin Density Approximation (LSDA) [55] as in Ref. [32] for supercells containing 4 or 8 formula units of CeO_2. The same LMTO method has been successfully applied previously to study the effect of doping copper oxide high temperature superconductors [21, 56]. Here, empty spheres were inserted in the interstitial region opposite to the oxygen atoms, a total of 16 or 32 spheres per supercell. Defective ceria CeO_x configurations were modeled with the supercell method by considering two concentrations: $x = 1.75$ and $x = 1.875$, in the 16 and 32 atom supercells, respectively.[57] The converged self-consistent results were obtained using a mesh of 286 or 89 k-points within the irreducible Brillouin zone for the small and large supercells, respectively. These calculations were made for a lattice constant a_0 of 5.45 Å for stoichiometric CeO_2 and 5.54 Å when vacancies are present. The atomic sphere radii in the LMTO calculations are $0.303a_0$ for Ce, $0.230a_0$ for O and $0.196a_0$ for the empty spheres. A precise tetrahedron method was used to determine the density-of-states (DOS) [58].

In order to calculate the XAS threshold energy, we start with the electronic structure obtained within the LMTO method. Our approach for modeling XAS [59] assumes that the absorption is essentially a screened single-particle process. A step to account for many-body relaxation effects is to extract an electron from the core shell and add it into the valence states. The electronic structure computations were carried out self-consistently under these constrained conditions. After the system has relaxed, we consider the total energy difference between the unperturbed state and the relaxed state to determine the XAS threshold energy.

The calculation of the excitation energy in x-ray photoemission spectroscopy (XPS) from the occupied Ce-f state is made in the same way as in our earlier study of Nd_2CuO_4 [32]. Excitation energies for localized f-electrons are different from those for itinerant electrons, since relaxation effects are smaller for itinerant bands. An electron is removed at an energy lying just below the Fermi level from the occupied majority state on one of the Ce atoms, and it is then spread out uniformly over the cell to account for a final state at high energy. The difference in total energy per electron between this state and the ground state gives the relaxation energy, $\Delta\epsilon$ defined in Appendix A. In particular, the final state will appear shifted by an amount $\Delta\epsilon$ with respect the Fermi level. The procedure for simulating inverse photoemission (or bremsstrahlung isocromat spectroscopy, BIS) is reversed. The final state then has one f-electron in an empty Ce-f state and the same amount of opposite neutralizing charge is spread uniformly over the cell. These procedures assume large excitation energies because the compensating uniform charges are valid approximations for free electron states ignoring the lattice potential [60].

III. RESULTS

A. Ground-state properties

The VASP calculation on a Ce_4O_8 cell gives an equilibrium lattice constant $a_0 = 5.466$ Å and a bulk modulus $B_0 = 198.9$ GPa, which compare well with the corresponding low-temperature experimental values $a_0 = 5.41$ Å [61] $B_0 = 204$ GPa [62]. By removing an oxygen atom and by letting the volume and the atomic positions relax, the lattice constant was found to expand to $a = 5.507$ Å , the bulk modulus reduced to $B = 155.9$ GPa, and the total spin magnetic moment was 2 μ_B. This predicted ferromagnetic structure is consistent with experiments [63–65] and other first principles studies [66]. We note that by removing all the oxygen atoms, one recovers the fcc-phase of Ce, and the calculated bulk modulus is only 51.4 GPa for the non-magnetic α phase at an equilibrium lattice constant of 4.714Å. Our results for Ce_4O_{8-N} as a function of the number N of oxygen vacancies are summarized in Fig. 1. The calculated chemical expansion coefficient of $CeO_{2-\delta}$ is given by $\alpha_c = (a - a_0)/(a_0\delta)$. However, our results for O-vacancies in the small unit cell Ce_4O_{8-N} show that α_c is not at all linear. In fact, between $N = 0$ and $N = 1$, α_c is 0.03, while between $N = 3$

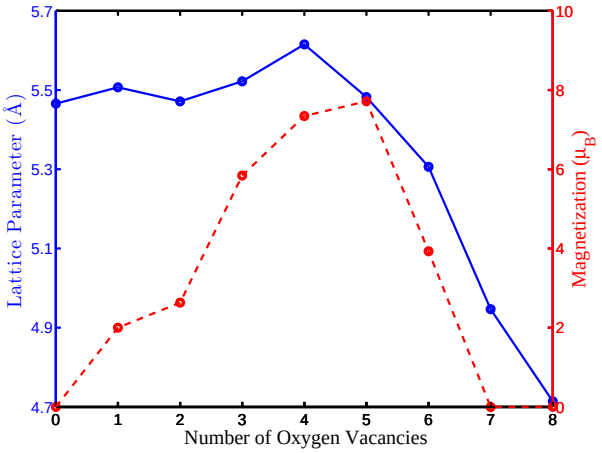

FIG. 1. (Color online) Lattice constant (points connected by solid line) and magnetic moment (points connected by dashed line) results of the VASP based calculations on a Ce_4O_{8-N} cell as function of the number N of oxygen vacancies. Both volume and atomic positions were relaxed while keeping the cubic symmetry. For each N the configuration with the lowest energy was chosen.

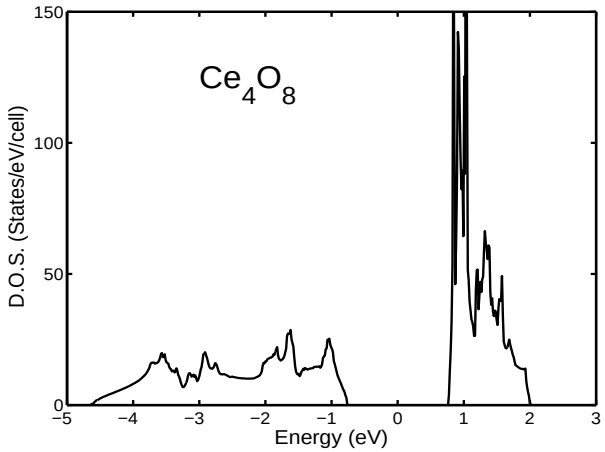

FIG. 2. Total DOS for Ce_4O_8 calculated from 286 k-points. The Fermi level is at zero.

and $N = 4$, $\alpha_c = 0.07$, which is slightly below the experimental value $\alpha_c = 0.08 - 0.1$ [30]. Part of the anomalous behavior of $\alpha_c = 0.07$ can be explained in term of oxygen vacancy ordering leading to lattice contractions opposite to the chemical expansion[67]. The GGA calculation for one vacancy in a large $2 \times 2 \times 2$ supercell with 95 atoms gives a larger dilute vacancy limit ($\delta \to 0$) $\alpha_c = 0.05$ as shown by Marrocchelli *et al.*. Therefore, calculated values of α_c are not easy to compare with experiment within large ranges of T and δ. The discrepancy between DFT and the experiment could be explained by disorder and entropy effects leading to larger high-temperature equilibrium volumes [29]. The electronic entropy will increase the lattice constant of oxygen-deficient ceria, since the DOS near the Fermi level is higher at large volume and large δ, although this effect is rather weak. Lattice disorder is caused both by zero-point motion [31] and thermal vibrations [68], which produce a pressure given by $d\omega/dV$, where the phonon frequency ω is proportional to $\sqrt{aB}$. Also the effect of spin and orbital magnetic fluctuations usually produce lattice expansions as shown in Ref. [29]. The relevant temperature range for catalytic applications is rather high (i.e. $500-700$ °C) [49] and the effects from lattice vibrations on magnetic fluctuations in this range make the total entropy balance complicated.

The LMTO electronic structure of CeO_2 is found to be non-magnetic and insulating as shown in Fig. 2. The distance between the valence band and the Ce $4f$ edge is about 1.6 eV, to be compared with 3 eV in experiments [27, 69]. Ferromagnetism (FM) is not expected because of the absence of occupied Ce $4f$ electrons. An oxygen atom has 4 valence p electrons. But all 3 O-$2p$ bands are below E_F and can harbor 6 electrons (2 spins in each band). Therefore, each removal of an O-atom removes 3 occupied p-bands, but since the system has only 4 fewer electrons, this means that E_F will rise, and one more band will be occupied to account for the two additional electrons. Thus, an oxygen vacancy introduces partially filled Ce f states and the FM ordering sets in because the high DOS of Ce-f states produces a Stoner exchange splitting. The calculated moment is 0.52 μ_B per Ce atom in $CeO_{1.75}$ and the FM state has a lower total energy (E_{tot}) than the non-magnetic state by 0.14 eV per formula unit. The induced moment per oxygen is negative, about 0.01 μ_B, and the total moment per Ce_4O_7 cell is exactly 2.0 μ_B, or 0.50 μ_B per $CeO_{1.75}$ unit. The FM state is half-metallic with no minority bands at E_F, and as expected from the qualitative discussion above, the charge transfer to the majority states is exactly 2 spin states per cell, see Figs. 3 and 4. Consequently, there also are exactly 2 more majority states than minority states in the calculation for the 32-site cell Ce_8O_{15}, which corresponds to $CeO_{1.875}$. Here there are two types of Ce sites, the 4 closest to the O-vacancy, Ce_v, has each a moment of 0.33 μ_B and the 4 towards the interior, Ce_i, have 0.19 μ_B each [70]. Together with the small negative moments on the oxygen this gives exactly 2.0 μ_B per Ce_8O_{15} cell, or 0.25 μ_B per $CeO_{1.875}$ unit. In other words, the removal of one oxygen atom gives rise to a spin magnetic moment of $2\mu_B$ in the dilute vacancy limit ($\delta \to 0$).

B. Excited-state properties

Table I compares measured positions of several Kohn-Sham core energy levels with the corresponding calculated XAS threshold energies. Clearly, the total energy calculations give XAS threshold energies in much better agreement with experiments [65, 71, 72] compared to just taking the Kohn-Sham energy of the core level relative to E_F. Note that we are not looking for absolute

values, but rather for relative differences between FM and non-magnetic configurations with or without vacancies. In particular, the value of the Ce M-edge threshold is reduced by about 1 eV for an oxygen vacancy in the small supercell Ce_4O_7 and this value is consistent with the displacements of the Ce_2O_3 [72] and of the metallic Ce [71] threshold energies toward lower values. In the large super-cell, Ce_8O_{15}, the Ce-3d Kohn-Sham core levels differ by 0.44 eV between the two types of Ce sites. The threshold of oxygen K-edge position seems less affected by the formation of O vacancies in ceria in agreement with measurements performed in oxygen-deficient CeO_2 nanoparticles [65].

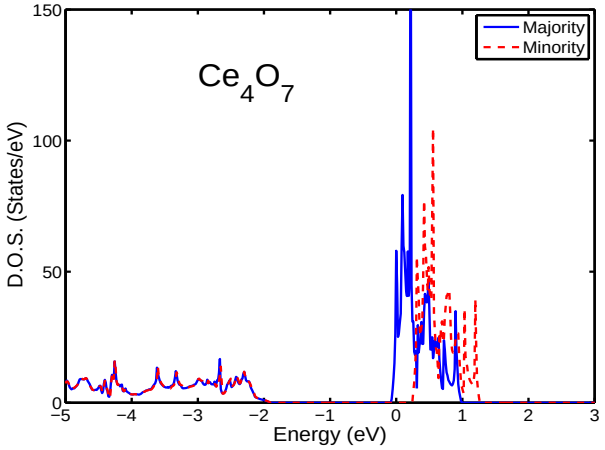

FIG. 3. (Color online) Total spin-polarized DOS for Ce_4O_7 calculated from 286 k-points using the LSDA. The Fermi level is at zero.

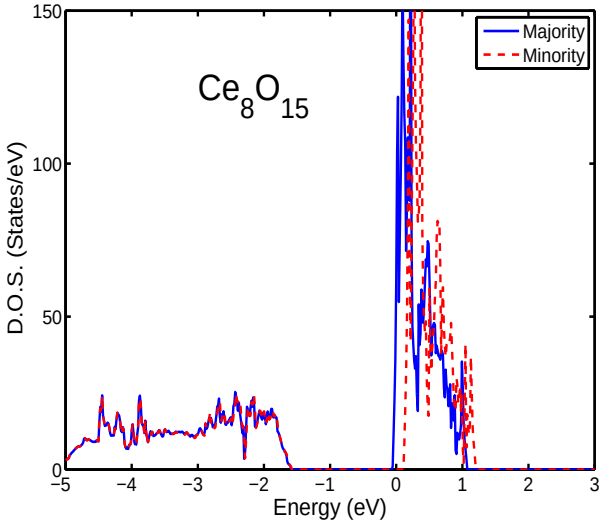

FIG. 4. (Color online) Total spin-polarized DOS for Ce_8O_{15} calculated from 89 k-points using the LSDA. The Fermi level is at zero.

TABLE I. Core level Kohn-Sham energies (ϵ) and the calculated threshold energies (E_{XAS}) for x-ray absorption for the upper spin-orbit Ce-$d_{5/2}$ state (M_5-level) and O-1s state (K-level), all in units of eV. The spin polarized potentials V^σ produced by magnetic valence (non-relativistic) electrons affect the position of the M_5-level. (E_F for the insulating Ce_4O_8 is assumed to be in the middle of the gap of 1.54 eV.) The calculated Ce-3d spin-orbit splitting is 18.82 eV.

core hole	$(E_F-\epsilon)$	E_{XAS}	experiment
Ce-3$d_{5/2}$ in Ce_4O_8	856.2	871.6	877 Ref. [71]
O-1$s_{1/2}$ in Ce_4O_8	501.0	523.7	528 Ref. [65]
Ce-3$d_{5/2}$-maj. in Ce_4O_7	856.0	870.8	
Ce-3$d_{5/2}$-min. in Ce_4O_7	856.0	870.3	
O-1$s_{1/2}$ in Ce_4O_7	502.0	523.5	

The results for the XPS and BIS excitation energy per electron given in Table II show trends similar to those given in Ref. [32] for $Nd_{2-x}Ce_xCuO_4$. In particular, the relaxation corrections for defective ceria split the single f peak in LSDA to an occupied and an unoccupied f band. The former falls below and the latter lies above E_F. Our XPS calculations predict that the f occupied peak appears at about 1 eV below the Fermi level while experimentally the position of this peak seems to be even lower. Typical *in situ or in operando* Ce 4f and Ce 3d x-ray photoelectron spectra of a ceria electrode are shown in Fig. 3a of Ref. [49]. Figure 7 of Ref. [50] provides the spatially resolved spectral image of the Ce 4f valence band, allowing visualization of regions of electrochemical activity in a ceria electrode. In fact, the presence of Ce^{3+} species is revealed by the intensity of the Ce 4f occupied peak at about 2 eV binding energy as already demonstrated by *ex situ* results [73]. The Ce 3d XPS core-level spectra display different final-state populations of 4f, which lead to the peak splitting shown in Fig. 3b of Ref. [49]. The final state effects lead to an upward shift of the lowest binding Ce-3$d_{5/2}$ peak attributed to the Ce^{3+} state [see also Ce 3d XPS spectra in Fig.1 of Ref. [73]], which is consistent with the shift of the calculated Ce 3$d_{5/2}$ XAS threshold [74] given in Table I.

For the smaller unit cell, Ce_4O_7, where all the Ce atoms are equivalent, we find that the occupied f band shifts only by -0.7 eV, indicating that the degree of localization of the f orbital plays an important role in the value of the energy shift. If we take the atomic positions relaxed by VASP, the energy shift becomes -0.8 eV. Therefore, the correction due to atomic relaxation is of the order of 0.1 eV. Calculations were also made for the large cell, Ce_8O_{15}, where both Ce_v and Ce_i give the same position for the f occupied peak at about 1 eV below E_F [79]. This is consistent with the observation that the Ce 4f binding energy does not change much with the vacancy concentration, but that different contributions from different sites lead to some broadening. Therefore, the excess electrons left behind by the removal of neutral oxygen atoms produce occupied f states with

practically the same 2 eV binding energy. The reason for the underestimation of the theoretical XPS relaxation is not known, but several mechanisms may be involved. As shown above, part of the correction is due to lattice relaxation near the vacancies. Other possible modifications of the Ce potential would result at surface sites or due to atomic vibrations. Interestingly, the calculated shift for the f states in $Nd_{2-x}Ce_xCuO_4$ [32] has also been found to be about 2 eV. It is also possible that the approximation of a completely delocalized excited state is less appropriate for Ce at these energies.

TABLE II. Calculated relaxation, $\Delta\epsilon$, of Ce-f states in XPS and BIS in eV.

excitation	Ce in Ce_4O_7	Ce_v in Ce_8O_{15}	Ce_i in Ce_8O_{15}
XPS	-0.7	-1.0	-1.1
BIS	1.0	1.1	1.0

IV. CONCLUSIONS

We have obtained electronic structures of supercells of $CeO_{2-\delta}$ within the framework of the DFT. The experimental equilibrium lattice constants, bulk moduli and magnetic moments are well reproduced by the generalized gradient approximation (GGA) without the need to introduce a large Coulomb parameter U. The computed value of lattice chemical expansion α_c as a function of O-vacancy concentration is not linear for δ ranging from 0 to 1. Pristine CeO_2 is found to be a non-magnetic insulator with magnetism setting in as soon as oxygens are removed from the structure. Excitation properties are simulated via constrained total energy calculations, and Ce-M and O-K edge x-ray absorption threshold energies are discussed. Our study shows that the way the ground state is probed by different spectroscopies can be modified significantly through final state effects. [32] In particular, these relaxation effects yield a renormalization of f-levels away from the Fermi Level for electron excitation spectroscopies. Our result that f electrons reside near the Fermi level in the ground state of oxygen deficient ceria is crucial for understanding catalytic properties of CeO_2 and related materials.[26].

ACKNOWLEDGMENTS

We acknowledge useful discussions with Dario Marrocchelli. The work at Northeastern University is supported by the US Department of Energy (USDOE) Contract No. DE-FG02-07ER46352. The Advanced Light Source is supported by the Director, Office of Science, Office of Basic Energy Sciences, of the USDOE under Contract No. DE-AC02-05CH11231. We benefited from computer time from Northeastern University's Advanced Scientific Computation Center (ASCC) and USDOEs NERSC supercomputing center.

Appendix A: Details of Constrained DFT Computations

In the XPS final state, one whole electron is transferred from the ground-state to a homogeneous plane-wave single-particle state. We can simulate this process by creating a hole obtained by removing states from the local DOS (LDOS) over a narrow energy window $[E_1, E_F^*]$, where E_F^* is the Fermi energy in the excited state and $E_1 \leq E_F^*$ is a cut-off energy. The electronic density $\rho_h(r)$ associated with the hole at the site t is

$$\rho_h(r) = \sum_\ell \int_{E_1}^{E_F^*} N_{t,\ell}^*(E) R_{t,\ell}^2(E,r) dE \qquad \text{(A1)}$$

Here, $N_{t,\ell}^*(E)$ is the self-consistent LDOS and $R_{t,\ell}(E,r)$ is the radial wave function component at the site t with angular momentum ℓ. The total electron density $\rho^*(r)$ for the excited state thus is

$$\rho^*(r) = \sum_{t',\ell} \int_{-\infty}^{E_F^*} N_{t',\ell}^*(E) R_{t',\ell}^2(E,r) dE - \rho_h(r) + \frac{1}{\Omega}, \qquad \text{(A2)}$$

where the last term in Eq. A2 imposes charge neutrality within the simulation cell of volume Ω.

The charge density in the final state $\rho^*(r)$ allows us to determine the total energy E^* of the excited state. The electrostatic and exchange-correlation contributions are evaluated straightforwardly from $\rho^*(r)$. The kinetic energy corresponding to the excited charge density does not involve a single energy level of the solid but rather a group of states and it can be calculated using the standard expression given by Janak [75], which involves the Kohn-Sham energy average

$$\epsilon^* = \sum_\ell \int_{E_1}^{E_F^*} N_{t,\ell}^*(E) E dE. \qquad \text{(A3)}$$

In this way, the total energy E^* can be obtained in terms of the Kohn-Sham energy average ϵ^* and the hole density ρ_h exactly as in the XAS threshold energy calculations within the Δ self-consistent-field (ΔSCF) method [59, 76]. Finally, the energy $\mathcal{E}$ of the XPS photoelectron is given by [77]

$$\mathcal{E} = \hbar\omega + (E_0 - E^*) - E_F^*, \qquad \text{(A4)}$$

where $\hbar\omega$ is the photon energy, E_0 is the ground state energy, and E_F^* is the Fermi level for the excited state. If Koopmans theorem applies

$$\mathcal{E} = \hbar\omega + \epsilon - E_F, \qquad \text{(A5)}$$

where the Kohn-Sham energy average

$$\epsilon = \sum_{\ell} \int_{E_1}^{E_F} N_{t,\ell}(E) E dE \qquad \text{(A6)}$$

is calculated in the ground state. The difference between Eq. A4 and Eq. A5 defines the relaxation energy $\Delta\epsilon$. DFT is expected to give a reasonable description of the energy difference $\Delta\epsilon$ involved in the photoemission process[78].

In order to focus on the excitation corresponding to a given DOS peak, in actual computations, we considered a narrow energy interval $[E_\beta, E_F^*]$ containing a fraction β of an electron per site t, and renormalized the result to obtain $\Delta\epsilon(\beta)/\beta$ to account for a whole electron involved in the XPS process [79]. We have performed test computations using a range of β values and found that the relaxation energy is very insensitive to the value of β used, which is also anticipated from the analysis of Ref. [80]. Note that placing the hole on only one of the sites in the unit cell is an approximation for removing a band electron in that it neglects the overlap of the wave function with neighboring sites. This however is expected to be a reasonable approximation for localized f-electrons of interest here. To check this point, we computed the excitation energy self-consistently in Ce_4O_7 where we removed 1/4th of an f-electron from each of the 4 Ce atoms in the unit cell, i.e. a total of one electron from the unit cell. The value of the relaxation energy so obtained was 0.75 eV compared to 0.7 eV shown in Table II, which is within the intrinsic error of 0.05 eV in our total energy computations.

[1] A. Trovarelli, *Catalysis by Ceria and Related Materials*, Catalytic Science Series, vol. 2, (Imperial College Press, London, 2002).

[2] Friedrich Esch, Stefano Fabris, Ling Zhou, Tiziano Montini, Cristina Africh, Paolo Fornasiero, Giovanni Comelli, Renzo Rosei, Science **309**, 752 (2005).

[3] M. Veronica Ganduglia-Pirovano, Alexander Hofmann, Joachim Sauer, Surface Science Reports **62**, 219 (2007).

[4] A. Trovarelli, Cat. Rev. - Sci. Eng. **38**, 439-520 (1996).

[5] A. Atkinson, S Barnett, R.J. Gorte, J.T.S. Irvine, A.J. McEvoy, M.B. Mogensen, S Singhal, J. Vohs, Nature Mat. **3**, 17 (2004).

[6] Mogens Mogensen, Nigel M. Sammes, Geoff A. Tompsett, Solid State Ionics **129**, 63 (2000).

[7] E.P. Murray, T. Tsai, and S.A. Barnett, Nature **400**, 649 (1999).

[8] S. Park, J. M. Vohs and R. J. Gorte, Nature **404**, 265 (2000).

[9] J.B. Park, J. Graciani, J. Evans, D. Stacchiola, S. Ma, P. Liu, A. Nambu, J. F. Sanz , J. Hrbek, and J. A. Rodriguez, Proc. Natl. Acad. Sci. **163**, 4975 (2009).

[10] J. A. Rodriguez, S. Ma, P. Liu, J. Hrbek, J. Evans, M. Perez, Science **318**, 1757 (2007).

[11] M. V. Ganduglia-Pirovano, J. L. F. Da Silva and J. Sauer, Phys. Rev. Lett. **102**, 026101 (2009).

[12] Hui-Ying Li, Hai-Feng Wang, Xue-Qing Gong, Yang-Long Guo, Yun Guo, Guanzhong Lu, and P. Hu, Phys. Rev. B **79**, 193401 (2009).

[13] W. Lai and S. M. Haile, J. Am. Ceram. Soc. **88**, 2979-2997 (2005).

[14] C. Lu, W. L. Worrell, J. M. Vohs, and R. J. Gorte, J. Electrochem. Soc. **150**, A1357-A1359 (2003).

[15] Chunjuan Zhang, Michael E. Grass, Anthony H. McDaniel, Steven C. DeCaluwe, Farid El Gabaly, Zhi Liu, Kevin F. McCarty, Roger L. Farrow, Mark A. Linne, Zahid Hussain, Gregory S. Jackson, Hendrik Bluhm and Bryan W. Eichhorn, Nature Mat. **9**, 944 (2010).

[16] S. Adler, Chem. Rev. **104**, 4791 (2004).

[17] W.C. Chueh, H. Yong, W. Jung, and S. M. Haile, Nature Mater. 11, **155** (2012).

[18] B. Murugan and A. V. Ramaswamy, J. Am. Chem. Soc. **129**, 3062 (2007).

[19] M. Nolan, S. Parker, and G. W. Watson, Phys. Chem. Chem. Phys. **8**, 216(2005).

[20] T. X. T. Sayle, S. C. Parker, and C. R. A. Catlow, Surf. Sci. **316**, 329 (1994).

[21] T. Jarlborg, B. Barbiellini, R.S. Markiewicz and A. Bansil, Phys. Rev. B **86**, 235111, (2012); T. Jarlborg, A. Bianconi, B. Barbiellini, R.S. Markiewicz, A. Bansil, J. Supercond. Nov. Magn. **26**, 2597 (2013).

[22] Matthew B. Watkins, Adam S. Foster, and Alexander L. Shluger, J. Phys. Chem. C **111**, 15337 (2007).

[23] Natasha M. Galea, David O. Scanlon, Benjamin J. Morgan, Graeme W. Watson, Molecular Simulation **35**, 577 (2009). DOI 10.1080/08927020802707001

[24] Konstanze R. Hahn, Marcella Iannuzzi, Ari P. Seitsonen, and Jürg Hutter, J. Phys. Chem. C **117**, 1701 (2013).

[25] O.Hellman, N.V.Skorodumova, and S.I.Simak, Phys. Rev. Lett. **108**, 135504 (2012).

[26] B. Hammer and J.K. Norskov, Advances in Catalysis **45**, 71 (2000).

[27] N. V. Skorodumova, R. Ahuja, S. I. Simak, I. A. Abrikosov, B. Johansson, and B. I. Lundqvist, Phys. Rev. B **64**, 115108 (2001).

[28] N.V. Skorodumova, S. I. Simak, B. I. Lundqvist, I. A. Abrikosov, and B. Johansson, Phys. Rev. Lett. **89**, 166601 (2002).

[29] T. Jarlborg, E.G. Moroni and G. Grimvall, Phys. Rev. B **55**, 1288, (1997).

[30] Dario Marrocchelli, Sean R. Bishop, Harry L. Tuller, Graeme W. Watson and Bilge Yildiz, Phys. Chem. Chem. Phys. **14**, 12070 (2012).

[31] B. Barbiellini, E. G Moroni, T. Jarlborg Journal of Physics: Condensed Matter **2**, 7597 (1990);

[32] T. Jarlborg, B. Barbiellini, H. Lin, R. S. Markiewicz, and A. Bansil, Phys. Rev. B **84**, 045109 (2011).

[33] A. N. Chantis, M. van Schilfgaarde, and T. Kotani, Phys. Rev. B **76**, 165126 (2007).

[34] B. Barbiellini and A. Bansil, J. Phys. Chem. Solids **66**, 2192 (2005).

[35] M. Cococcioni and S. de Gironcoli, Phys. Rev. B **71**, 035105 (2005).

[36] D. A. Andersson, S. I. Simak, B. Johansson, I. A. Abrikosov, and N. V. Skorodumova, Phys. Rev. B **75**,

035109 (2007).
[37] C. W. M. Castleton, J. Kullgren, and K. Hermansson, J. Chem. Phys. **127**, 244704 (2007).
[38] Christoph Loschen, Javier Carrasco, Konstantin M. Neyman, and Francesc Illas, Phys. Rev. B **75**, 035115 (2007).
[39] Talgat M. Inerbaev, Sudipta Seal, Artëm E. Masunov, J. Mol. Model. **16**, 1617 (2010).
[40] Gloria Preda and Gianfranco Pacchioni, Catalysis Today **177**, 31 (2011).
[41] Christian Spiel, Peter Blaha, Yuri Suchorski, Karlheinz Schwarz, and Günther Rupprechter, Phys. Rev. B **84**, 045412 (2011).
[42] Amra Peles, J. Mater. Sci. **47**, 7542 (2012). DOI 10.1007/s10853-012-6423-1
[43] Hong Jiang, Ricardo I. Gomez-Abal, Patrick Rinke, and Matthias Scheffler, Phys. Rev. Lett. **102**, 126403 (2009).
[44] L. Gerward, J. Staun Olsen, L. Petit, G. Vaitheeswaran, V. Kanchana and A. Svane, Journal of Alloys and Compounds **400**, 56 (2005).
[45] Jesus Graciani, Antonio M. Marquez, Jose J. Plata, Yanaris Ortega, Norge C. Hernandez, Alessio Meyer, Claudio M. Zicovich-Wilson, and Javier Fdez. Sanz, J. Chem. Theory Comput. **7**, 56 (2011).
[46] Roland Gillen, Stewart J. Clark, and John Robertson, Phys. Rev. B **87**, 125116 (2013).
[47] Michael E. Grass, Patrik G. Karlsson, Funda Aksoy, Mans Lundqvist, Bjorn Wannberg, Bongjin S. Mun, Zahid Hussain, and Zhi Liu, Review of Scientific Instruments **81**, 053106 (2010).
[48] Funda Aksoy, Michael E. Grass, Sang Hoon Joo, Naila Jabeen, Young Pyo Hong, Zahid Hussain, Bongjin S. Mun and Zhi Liu, Nuclear Instruments and Methods in Physics Research Section A: Accelerators, Spectrometers, Detectors and Associated Equipment **645**, 260 (2011).
[49] William C. Chueh, Anthony H. McDaniel, Michael E. Grass, Yong Hao, Naila Jabeen, Zhi Liu, Sossina M. Haile, Kevin F. McCarty, Hendrik Bluhm, and Farid El Gabaly, Chemistry of Materials **24**, 1876 (2012).
[50] Chunjuan Zhang, Michael E. Grass, Yi Yu, Karen J. Gaskell, Steven C. DeCaluwe, Rui Chang, Gregory S. Jackson, Zahid Hussain, Hendrik Bluhm, Bryan, W. Eichhorn and Zhi Liu, ACS Catal. **2**, 2297 (2012).
[51] G. Kresse and D. Joubert, Phys. Rev. B **59**, 1758 (1999).
[52] G. Kresse, G and J. Furthmuller, Phys. ReV. B **54**, 11169 (1996); G. Kresse and J. Hafner, Phys. Rev. B **48**, 13115 (1993).
[53] J. P. Perdew, K. Burke and M. Ernzerhof, Phys. Rev. Lett. **77**, 3865 (1996).
[54] O.K. Andersen, Phys. Rev. B**12**, 3060 (1975); B. Barbiellini, S.B. Dugdale and T. Jarlborg, Comput. Mater. Sci. **28**, 287 (2003).
[55] W. Kohn and L.J. Sham, Phys. Rev. **140**, A1133 (1965); O. Gunnarsson and B.I Lundquist, Phys. Rev. B **13**, 4274 (1976).
[56] B. Barbiellini and T. Jarlborg, Phys. Rev. Lett. **101**, 157002 (2008).
[57] Non-stoichometric compositions could be investigated via first-principles KKR-CPA methodology: A. Bansil, S. Kaprzyk, P.E. Mijnarends and J. Tobola, Phys. Rev. B **60**, 13396 (1999); A. Bansil, Phys. Rev. B20, 4025(1979); A. Bansil, Phys. Rev. B20, 4035(1979); L. Schwartz and A. Bansil, Phys. Rev. B **10**, 3261 (1974).
[58] J. Rath and A.J. Freeman, Phys. Rev. B **11**, 2109 (1975).
[59] P. Lerch, T. Jarlborg, V. Codazzi, G. Loupias and A.M. Flank, Phys. Rev. B**45**, 11481 (1992).
[60] T. Jarlborg and P.O. Nilsson, J. Phys. **C 12**, 265 (1979).
[61] L. Eyring, in Handbook on the Physics and Chemistry of Rare Earths, edited by K. A. Gschneider and L. Eyring (North- Holland, Amsterdam, 1979), Vol. 3, Chap. 27.
[62] A. Nakajima, A. Yoshihara, and M. Ishigame, Phys. Rev. B **50**, 13 297 (1994).
[63] V. Fernandes, R. J. O. Mossanek, P. Schio, J. J. Klein, A. J. A. de Oliveira, W. A. Ortiz, N. Mattoso, J. Varalda, W. H. Schreiner, M. Abbate, and D. H. Mosca, Phys. Rev. B **80**, 035202 (2009).
[64] V. Fernandes, P. Schio, A. J. A. de Oliveira, W. A. Ortiz, P. Fichtner, L. Amaral, I. L. Graff, J. Varalda, N. Mattoso, W. H. Schreiner and D. H. Mosca, J. Phys.: Condens. Matter bf 22, 216004 (2010).
[65] Shih-Yun Chen, Yi-Hsing Lu, Tzu-Wen Huang, Der-Chung Yan and Chung-Li Dong, J. Phys. Chem. C **114**, 19576 (2010).
[66] Xiaoping Han, Jaichan Lee, and Han-Ill Yoo, Phys. Rev. B **79**, 100403 R (2009).
[67] Y. Kuru D. Marrocchelli, S. R. Bishop, D. Chen, B. Yildiz, and H. L. Tuller, Journal of The Electrochemical Society **159** F799 (2012).
[68] T. Jarlborg, Phys. Rev. B**59**, 15002, (1999).
[69] E. Wuilloud, B. Delley, W.-D. Schneider and Y. Baer, Phys. Rev. Lett. **53**, 202 (1984).
[70] The valence charge is 0.05 electrons larger on the Ce with small moment compared to the other Ce site.
[71] O. Yagci, J. Phys. C: Solid State Phys. **19** 3487 (1986).
[72] C. L. Melcher, S. Friedrich, M. A. Spurrier, P. Szupryczynski, R. Nutt, Nuclear Science, IEEE Transactions on **52**, 1809 (2005). DOI 10.1109/TNS.2005.856594
[73] D.R. Mullins, P.V. Radulovic, S.H. Overbury, Surface Science **409**, 307 (1998).
[74] We should keep matrix element effects in mind in comparing theoretical and experimental spectral intensities in various highly resolved spectroscopies. See, e.g., R. S. Markiewicz and A. Bansil, Phys. Rev. Lett. **96**, 107005 (2006); J. Nieminen, H. Lin, R. S. Markiewicz, and A. Bansil, Phys. Rev. Lett. **102**, 037001 (2009); J. Mader, S. Berko, H. Krakauer and A. Bansil, Phys. Rev. Letters 37, 1232(1976); A. Bansil, M. Lindroos, S. Sahrakorpi, and R. S. Markiewicz, Phys. Rev. B **71**, 012503 (2005).
[75] J.F. Janak, Phys. Rev. B **12**, 7165 (1978).
[76] L. Hedin and A. Johansson, J. Phys. B **2**, 1336 (1969).
[77] Takashi Fujikawa, J. Phys. Soc. Japan **51**, 2619 (1982).
[78] I. Dabo, A. Ferretti, N. Poilvert, Y. Li, N. Marzari, and M. Cococcioni, Phys. Rev. B **82**, 115121 (2010).
[79] This does not mean that we are exciting a fraction of an electron β since each Bloch electron is spread over a macroscopic number of unit cells in the crystal, and its spectral weight on any atom is negligibly small. All results in Table II are based on using β in between 0.125 and 0.45.
[80] L. Ley, F. R. McFeely, S. P. Kowalczyk, J. G. Jenkin, and D. A. Shirley, Phys. Rev. B **11**, 600 (1975); S. P. Kowalczyk, L. Ley, R. L. Martin, F. R. McFeely, and D. A. Shirley, Faraday Discuss. Chem. Soc. **60**, 7 (1975).